ELSEVIER

Biophysical Chemistry 69 (1997) 221–232

Biophysical Chemistry

# Secondary structure of an isolated P-region from the voltage-gated sodium channel: a molecular modelling/dynamics study

Pascal Cosette [a], Ian D. Kerr [b], Paolo La Rocca [b], Hervé Duclohier [a,1], Mark S.P. Sansom [b,*]

[a] *UMR 6522 CNRS-Université de Rouen (IFRMP 23), Boulevard M. de Broglie, Mont-Saint-Aignan 76821, France*

[b] *Laboratory of Molecular Biophysics, The Rex Richards Building, University of Oxford, South Parks Road, Oxford OX1 3QU, UK*

Received 13 January 1997; revised 8 July 1997; accepted 8 July 1997

**Abstract**

Conformational studies of synthetic peptides corresponding to the pore-forming regions of voltage-gated sodium channels show a high tendency for β-sheet conformation when interacting with lipid vesicles, as revealed by circular dichroism and infrared spectroscopy. These observations have guided our choice of possible molecular models for the P-region peptide of domain II of voltage-gated sodium channels: three alternative β-hairpins, with differing turn assignments, or an α-helical hairpin. After generation of models by distance geometry-based methods, molecular dynamics (MD) simulations were run, in the absence of explicit solvent molecules but employing three different dielectric constants, to explore possible conformational preferences. The simulations in the different dielectric environments suggest that a 4-residue turn with the sequence LCGE yields more stable β-hairpins. The MD results suggest that the SS1 part of the peptide may be more stable as an α-helix, whereas the SS2 part tends to adopt a β-conformation. © 1997 Elsevier Science B.V.

*Keywords:* Circular dichroism; Molecular modelling; Synthetic peptides; Pore-region; Sodium channel

## 1. Introduction

Voltage-gated sodium channels are proteins involved in the transmission of electrical signals along excitable membranes, and specifically for the rising phase and propagation of action potentials [1]. Although much is known about the electrophysiological importance of these proteins and their pharmacological properties (as recently reviewed [2]), their three-dimensional structures remain undetermined. After the determination of their primary structures [3], analysis of hydrophobicity profiles [4] allows the definition of four homologous domains (I to IV, with homology around 60%), each of which is composed of five hydrophobic segments (S1, S2, S3, S5 and S6), a highly charged segment S4 which is the main voltage sensor component [5], and a loop between S5 and S6 referred to as the P-region, (also H5 or SS1-SS2). The P-region, which traverses the mem-

* Corresponding author. Tel.: +44-1865-275371; fax: +44-1865-275182; e-mail: mark@biop.ox.ac.uk

[1] Tel.: +33-2-35-14-67-05; fax: +33-2-35-14-67-04; e-mail: herve.duclohier@univ-rouen.fr


*PII* S0301-4622(97)00099-9

brane twice, is a primary component of the channel lining, responsible for the sensitivity to blockers and the ionic selectivity [6,7] of the channel. Several molecular models have been designed to explain the organisation of these transmembrane segments and their relationship to channel function [8–11]. While site-directed mutagenesis provides an extremely powerful tool to test relationships between sequence and function, it remains almost impossible to obtain high-resolution structural data for the entire channel protein. An alternative approach is the use of synthetic peptide fragments of channels. Structural data on synthetic peptides can be obtained e.g., by circular dichroism (CD) or 2D NMR [12,13], while functional properties can be derived from planar bilayer studies. Such data can be employed to discuss plausible models [14–17].

In a previous paper [18], we focused on synthetic peptides mimicking the P-regions of the voltage-gated sodium channel from an electric eel. Their secondary structure was characterized using circular dichroism and Fourier transform infrared spectroscopy in trifluoroethanol that yielded approximately equal contents for $\alpha$-helical and $\beta$-sheet conformations. Similar experiments carried out in the presence of phospholipid vesicles demonstrated a significant increase in the $\beta$-sheet content with a concomitant decrease in the content of $\alpha$-helix. The ability of these synthetic peptides to insert in planar lipid bilayers and form ion permeable channels was also investigated. The formation of well-defined conductance levels indicated that synthetic P-region peptides interact and self-assemble in lipid systems. Related work on sodium channel P-region peptides employed fluorescence energy transfer experiments to demonstrate the capacity of P-region peptides to co-assemble in lipid bilayers [19].

In the light of these results, we have investigated possible models of the secondary structure of a peptide with a sequence corresponding to the P-region of the second domain of the eel voltage-gated sodium channel, referred to as $P_{II}$ [3]. The $P_{II}$ peptide is modelled either as a membrane-spanning $\beta$-hairpin with three different turn lengths or as an $\alpha$-helical hairpin. Molecular dynamics simulations have been performed in different dielectric conditions reflecting the various environments in which CD data had been collected. The results are discussed in terms of secondary structural models for P-region peptides in isolation and within self-aggregated channel-forming motifs.

## 2. Methods

### 2.1. Programs

Model building and molecular dynamics simulations were carried out using Xplor V3.1 [20]. Distance geometry and simulated annealing (DG/SA) regularisation were performed with the PARALLHDG parameter set for all-hydrogen representations in distance geometry calculations. During Stage 4 refinement (see below) the CHARMM PARAM19 parameter set [21] was employed with apolar hydrogen atoms represented by extended heavy atoms. Models were displayed and examined using Quanta V4.0 (Molecular Simulations, Waltham, MA). Diagrams were drawn using Molscript [22]. Model stereochemistry was checked using Procheck [23].

### 2.2. Generation of structures

For each of the four configurations examined, 100 structures were generated by a four-stage modelling process, of which Stages 3 and 4 are similar to a previously described simulated annealing via restrained molecular dynamics method [24]. Each configuration was defined by two restraints files: (a) distance restraints file that determined the hydrogen bonding pattern for a given configuration; and (b) a torsion angle restraints file that determined the secondary structure. Restraints remained active during all four stages of model generation. Stage 1 of the procedure employed distance geometry to generate 100 structures defining coordinates for backbone and C$\beta$ atoms only. Such 'sub-embedding' requires only a molecular structure file (i.e., a description of the covalent structure), and the two restraints files to generate the structures. Stage 2 was a 'full-embedding' process in which coordinates for sidechain atoms were generated from the backbone and C$\beta$ atom structures generated above. Stage 3 is a simulated annealing regularisation of the structures produced in Stage 2. Briefly, during a burst of molecular dynamics (3 ps) at 2000 K, weights applied to

geometric energy terms (bond lengths, bond angles, and dihedrals restraints) were gradually increased to values of 1.0. The system was then cooled to 100 K in 50 K steps (total simulation time 3.8 ps), while a repulsive van der Waals term is gradually introduced.

Prior to further refinement, the 100 structures per configuration produced by Stage 3 were reduced to 20 structures by a selection of those models that exhibited the fewest dihedral angle and distance restraints violations. These models were refined in Stage 4, a short molecular dynamics run in which electrostatic effects were gradually introduced. Stage 4 consisted of cooling from 500 to 300 K over 4 ps, during which C$\alpha$ atoms were released from their initial positional restraints, and during which sidechain atomic partial charges of polar and charged residues were scaled up from 5% to 42% of their full values (as given in the PARAM19 parameter set). Structures were then subjected to 5 ps of unrestrained molecular dynamics at 300 K and 2000 steps of conjugate gradient energy minimisation. Each set of 20 structures was subjected to two independent runs of Stage 4, thus generating a final ensemble of 40 structures for each configuration.

### 2.3. Molecular dynamics

All 40 structures produced in the previous step were examined to select one structure from each ensemble for extended MD simulations (see results for selection). MD simulations were then performed, in the absence of explicit solvent molecules but employing different dielectric constants, approximating the different media in which the secondary structure of the peptide had been investigated experimentally. For each starting model, three simulations were run: (i) with a distance-dependent dielectric constant ($\varepsilon = r$), favouring short-range electrostatic interactions, and thus mimicking screening by water and counterions; (ii) with $\varepsilon = 2$, a 'hydrophobic' environment, as in the core of a lipid bilayer, which promotes polar interactions; and (iii) with $\varepsilon = 80$, a 'polar' environment, which weakens polar interactions.

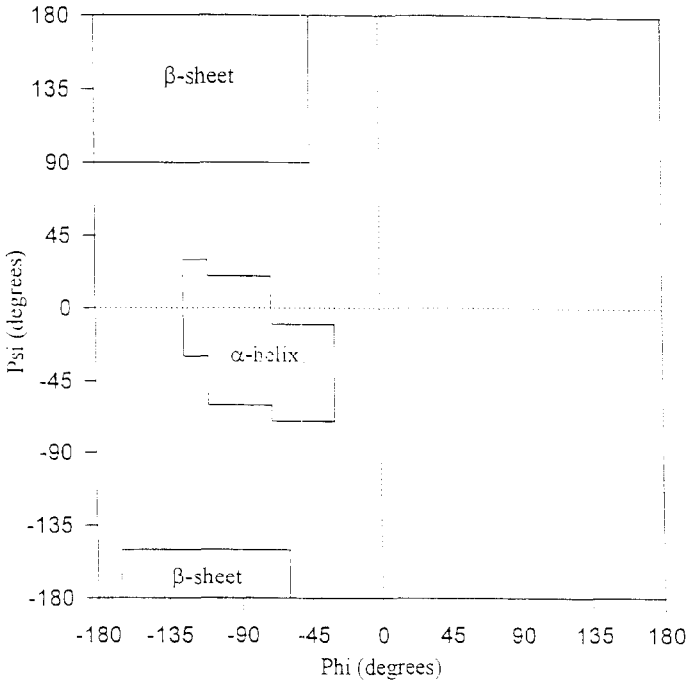


Fig. 1. Modified Ramachandran plot used to estimate conformational contents during MD. The $\alpha$- and $\beta$-conformational contents were measured from the Ramachandran plot occupancy residue by residue during the MD trajectories for structures saved every 1 ps.

Table 1
Definition of secondary structural models for the peptide $P_{II}$ and restraints applied during ensemble generation

| | β4 | β3 | β2 | α4 |
|---|---|---|---|---|
| Distance restraints | 9 – 26<br>11 – 24<br>13 – 22<br>15 – 20<br>20 – 15<br>22 – 13<br>24 – 11<br>26 – 9<br>} $d = 1.92 \pm 0.2$ Å | 9 – 25<br>11 – 23<br>13 – 21<br>15 – 19<br>19 – 15<br>21 – 13<br>23 – 11<br>25 – 9<br>} $d = 1.92 \pm 0.2$ Å | 11 – 26<br>13 – 24<br>15 – 22<br>17 – 20<br>20 – 17<br>22 – 15<br>24 – 13<br>22 – 11<br>} $d = 1.92 \pm 0.2$ Å | 6 – 10<br>7 – 11<br>8 – 12<br>9 – 13<br>10 – 14<br>11 – 15<br>20 – 24<br>21 – 25<br>22 – 26<br>23 – 27<br>24 – 28<br>25 – 29<br>} $d = 2.06 \pm 0.3$ Å |
| Dihedral angle restraints | 9-15 $\phi = -137 \pm 30°$<br>20-27 $\psi = +137 \pm 30°$ | 9-15 $\phi = -137 \pm 30°$<br>19-26 $\psi = +137 \pm 30°$ | 11-17 $\phi = -137 \pm 30°$<br>20-27 $\psi = +137 \pm 30°$ | 6-15 $\phi = -60 \pm 20°$<br>20-29 $\psi = -40 \pm 20°$ |

Secondary structural motifs are designated as follows: α4: helix-loop-helix; β2: β-hairpin with 2 residues in the loop (GE); β3: β-hairpin with a 3 residue loop (LCG); β4: β-hairpin with 4 residue loop (LCGE).
For distance restraints, a square-well potential with a force constant of 30 kcal $mol^{-1}$ $Å^{-1}$ is applied between the specified residues—the restraint operates between the carbonyl oxygen of the first residue and the amide hydrogen of the second.
For dihedral angle restraints, a force constant of 4 kcal $mol^{-1}$ $Å^{-1}$ operates for those residues in the desired conformation.
All restraints are given as the target value and allowable deviation.

MD was performed as described in previous studies [25]. Briefly, the system was heated to 300 K in 50 K steps over a period of 3 ps, followed by an equilibration of 22 ps during which velocities were rescaled, such that the effective simulation temperature remained in the window 290–310 K. The simulation phase consisted of 300 ps of unrestrained molecular dynamics during which the system was allowed to evolve freely. The distance and dihedral angle restraints employed in model generation (see above) were not applied during the MD simulations. For constant dielectric simulations, a shift-based cutoff of 14 Å was employed to truncate the nonbonded interactions, while in the $\varepsilon = r$ simulations a switching function between 5 and 9.5 Å was employed [26]. The timestep in the MD simulations was 0.2 fs with structures saved every 1 ps for subsequent analysis. To assess rigorously conformational content, saved structures were analyzed residue by residue in terms of percentage occupancy of the areas defined by the modified Ramachandran plot displayed in Fig. 1.

Table 2
Energetic and geometric analysis of the four different $P_{II}$ ensembles

| | Energy (kcal/mol) | | | | | RMSD (Å) |
|---|---|---|---|---|---|---|
| | $E_T$ | $E_{VDW}$ | $E_{ES}$ | $E_{NOE}$ | $E_{CDIH}$ | 'Core' region |
| β4 | −439 (18) | −127 (11) | −398 (10) | 0 (0.5) | 5 (5) | 1.7 |
| β3 | −412 (54) | −122 (18) | −393 (8) | 2 (7) | 12 (16) | 1.8 |
| β2 | −399 (33) | −117 (13) | −391 (9) | 1 (1) | 17 (12) | 1.8 |
| α4 | −504 (15) | −150 (9) | −423 (10) | 0 (0) | 0.5 (0.5) | 2.6 |

$E_T$: total potential energy; $E_{VDW}$: van der Waals energy; $E_{ES}$: electrostatic energy; $E_{NOE}$: energy associated with distance restraints; $E_{CDIH}$: energy associated with dihedral angle restraints.
RMSD: root mean square deviation of the ensemble for backbone atoms in the region where conformation was imposed ('core' region).
All energy values are mean (±sd) for 36 (β2) or 40 (β3, β4, α4) structures.

## 3. Results

### 3.1. Choice of configurations

The sequence modelled corresponds to that of the P-region of the second domain of the eel voltage-gated sodium channel [3]:

1 5 10 15 20 25 30

H-M-N-D-F-F-H-S-F-L-I-V-F-R-A-L-C-G-E-W-I-E-T-M-W-D-C-M-E-V-G

The sequence was blocked at the N-terminus by an acetyl group and at the C-terminus by a amide group to mimic the presence of peptide bonds at either end of the peptide when within the intact protein. In the native sodium channel, the P-region is believed to adopt a hairpin topology, with either end at the extracellular face of the membrane, and the centre of the P-region either at the intracellular face, or within the bilayer. Three configurations of possible $\beta$-hairpins were generated: with a 2, 3 or 4-residue turn in the centre of the P-region (models $\beta 2$, $\beta 3$, and $\beta 4$ respectively). A further model composed of a helix–loop–helix motif with a four-residue turn was also generated ($\alpha 4$). While this model is not supported by the circular dichroism data, it served as a control for the model-building and MD simulation studies. The choice of turn position and length within the sequence was determined on the basis of statistical analyses of high-resolution protein crystal structures [27,28]. Scanning the P-region sequence with a 4-residue window, we identify the tetrapeptide LCGE as the most likely candidate for the $\beta$-turn as determined by two independent propensity tables [27,28]. Thus, we selected GE, LCG and LCGE as the sequences of the turns within the $\beta 2$, $\beta 3$ and $\beta 4$ models respectively, with 8 residue $\beta$-strands on either side of the turn sequence. It should be noted for comparison that a previous analysis of the sequence of sodium channel P-region sequences suggested the tetrapeptide CGEW as the turn, i.e., a 1-residue shift from our definition [29]. The $\alpha 4$ model had LCGE as the turn sequence, with 10 residue $\alpha$-helices on either side.

Each configuration was defined by two restraints files (Table 1). A dihedral angle restraint file was employed to maintain the secondary structure of a given configuration, while a distance restraints file ensured that $\beta$-sheet hydrogen bonds or intrahelical ($i \leftarrow i + 4$) hydrogen bonds were maintained. Target values for restraints were taken from statistical analyses of proteins [30,31]. The combination of the two restraints files uniquely identifies a given configuration (Table 1).

### 3.2. DG / SA and SA / MD generated ensembles

Forty structures for each of the four configurations were generated as described. Geometric and energetic analyses are presented in Table 2. While most of the energy terms are comparable, there are a few differences that can be highlighted. The increased dihedral angle restraints energy ($E_{\mathrm{CDIH}}$) for the $\beta 2$ and $\beta 3$ ensemble occurs primarily due to restraints violations at residues proximal to the turn.

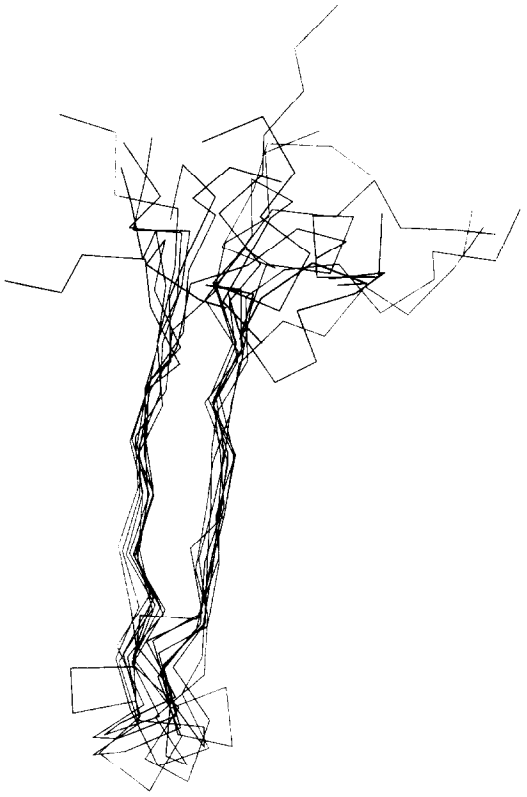

Fig. 2. Superimposition of 10 structures randomly selected from the ensemble $\beta 4$. The structures were superimposed using the C$\alpha$ atoms of the core region: from residue 10 to 16 for the first strand; and from residue 21 to 28 for the second. For clarity, only the C$\alpha$ are drawn.

reflecting the reduced conformational variability of shorter turns. The lower electrostatic energy (hence lower total energy) for the $\alpha 4$ ensemble is due to the larger number of hydrogen bond restraints in this ensemble compared to the $\beta$-hairpin ensembles (12 hydrogen-bonds for $\alpha 4$, 8 hydrogen-bonds for $\beta 2,3,4$; Table 1). The degree of variation within the ensembles is indicated by the root mean square deviation (RMSD) calculated over residues restrained in either $\alpha$-helical or $\beta$-strand conformation (Table 2) and is demonstrated by the superposition of structures for the $\beta 4$ ensemble in Fig. 2. While the three $\beta$-hairpin configurations have a similar RMSD value of 1.8 Å, the $\alpha 4$ ensemble has a larger RMSD (2.5 Å) reflecting the absence of restraints between the two $\alpha$-helices of the helical hairpin.

### 3.3. *Molecular dynamics simulations of selected structures*

The structure selected for extended MD simulations is shown for each of the four configurations in Fig. 3. Structures for MD were selected according to combined criteria: a low number of violations from the target restraints; acceptable backbone stereochemistry as assessed by the program Procheck [23]; and a low overall potential energy. Although the structures selected from the $\beta 2$, $\beta 3$ and $\beta 4$ ensembles have several violations of the dihedral angle restraints, the residues on which $\beta$-conformation was imposed (i.e., the 'core' residues) remained in the most preferred region of the Ramachandran plot, according to Procheck [32]. The structure selected

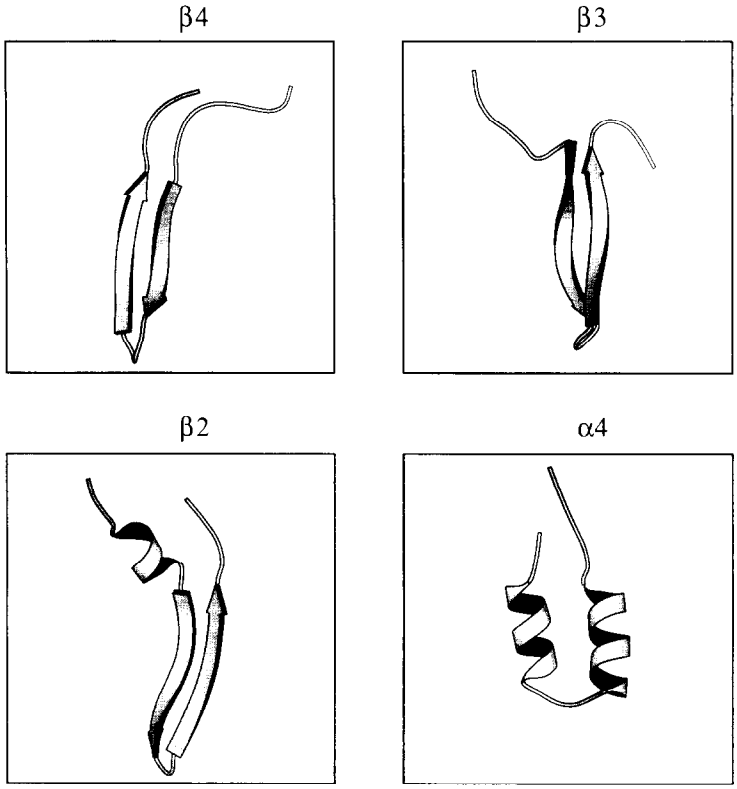


Fig. 3. Selected structures from the four ensembles: $\beta 4$, $\beta 3$, $\beta 2$ and $\alpha 4$. The structures were chosen from the simulating annealing via restrained molecular dynamics stage for their 'high' stereochemical quality. These were the starting structures for the subsequent 300 ps unrestrained molecular dynamics stage.

from the $\alpha 4$ ensemble exhibited only a single deviation from the target dihedral angle restraints. Notable in the $\beta 2$ preferred structure is the appearance of a short $\alpha$-helix from residues Asp-4 to Phe-9 (i.e., corresponding approximately to SS1), which was not imposed during the structure generation demonstrating the conformational flexibility permitted to the unrestrained regions of the peptide.

Molecular dynamics simulations were performed in isotropic environments using three different dielectric constants to mimic different solvent screening effects: $\varepsilon = 2$ and 80 for hydrophobic and highly screened environments, respectively, and $\varepsilon = r$ (i.e., a distance-dependent dielectric constant) for solvent screening of long-range interactions without affecting shorter range electrostatic effects. In assessing the simulations, we concentrate on the degree of retention of the original structure. This we have analysed in terms of the persistence of hydrogen bonds through the simulation, and in terms of the conformational persistence of residues. The simulations are discussed below with results presented in Table 3.

Table 3
Conformational analysis for the $P_{II}$ peptide during MD simulation

| | $\varepsilon$ | 'Core' region | | RMSD (Å) | H-bond index |
|---|---|---|---|---|---|
| | | $\alpha$ | $\beta$ | | |
| $\beta 4$ | $r$ | 3 (4) | 75 (7) | 1.3 | 0.51 |
| | 2 | 18 (6) | 53 (7) | 3.8 | 0.04 |
| | 80 | 15 (9) | 69 (9) | 3.8 | 0.11 |
| $\beta 3$ | $r$ | 8 (4) | 45 (9) | 4.1 | 0.02 |
| | 2 | 12 (5) | 51 (7) | 5.7 | 0.19 |
| | 80 | 24 (8) | 52 (7) | 4.8 | 0.03 |
| $\beta 2$ | r | 12 (3) | 58 (7) | 2.1 | 0.39 |
| | 2 | 4 (5) | 62 (6) | 3.2 | 0.21 |
| | 80 | 21 (6) | 61 (10) | 4.8 | 0.02 |
| $\alpha 4$ | r | 90 (5) | 0 (0) | 2.2 | 0.61 |
| | 2 | 52 (7) | 11 (4) | 2.5 | 0.44 |
| | 80 | 51 (7) | 28 (3) | 4.3 | 0.07 |

$\alpha$,$\beta$: % secondary structure (calculated over the 'core' region) averaged over the MD simulation.
RMSD values are calculated over C$\alpha$ atoms in the 'core' region during the last 100 ps of simulation.
H-bond index reflects the persistence of imposed H-bonds. A value of 1 signifies that all 'core' H-bonds remained throughout the simulation.

### 3.4. $\varepsilon = r$ simulations

The simulations using $\varepsilon = r$ for $\beta 4$ and $\alpha 4$ are shown in Figs. 4 and 5. It can be seen that from these two initial configurations, there is retention of the secondary structure throughout the MD simulation as reflected in the high-percentage secondary structural content for the core of the P-region (Fig. 5), and the high degree of persistence of hydrogen bonds for this region (Table 3). It is interesting to observe (Fig. 5) that for $\beta 4$, the C-terminal region (SS2) retains its $\beta$-conformation better than the N-terminal (SS1) region. On the contrary, for $\alpha 4$, the initial conformation appears more stable in SS1 than in SS2, with the evolution of a longer SS1 helix (Fig. 5B). Although for $\beta 3$ and $\beta 2$ the percentage secondary structure within the core remains high, the hydrogen bond persistence is considerably reduced. Indeed for $\beta 3$, all the hairpin hydrogen bonds are lost early in the simulation, the high RMSD for this simulation reflecting this, while for $\beta 2$, one hydrogen bond pair persists throughout the simulation while the other six are lost.

### 3.5. $\varepsilon = 2$ simulations

A dielectric constant of 2, mimicking a hydrophobic medium, was expected to preserve local electrostatic interactions such as intrahelical hydrogen bonds or antiparallel $\beta$-strands hydrogen bonds. However, the simulations starting from $\beta$ configurations did not conform to this expected pattern. Hydrogen bonds persisted only to a very small degree in the $\beta 2$ and $\beta 3$ simulations, and were lost completely in the first 25 ps of the $\beta 4$ simulation. Such absence of hydrogen bonds means that although a high percentage of the core residues remains in the $\beta$-strand region of the Ramachandran plot, there is no overall $\beta$-hairpin conformation. This increased flexibility is revealed in the markedly higher RMSD values for these simulations (Table 3). For the $\alpha 4$ simulation, the hydrogen bonds persisted to a greater degree (44%) than with $\beta$-hairpins, but both conformations are about equally maintained throughout the simulation (Table 3) with the same tendency noted above (in the case

of $\varepsilon = r$) for the SS1 helix to be more conserved than the SS2 helix.

### 3.6. $\varepsilon = 80$ simulations

Simulations in this high dielectric medium yielded similar results to those obtained in $\varepsilon = 2$. Hydrogen bond persistence was again very low for $\beta$-hairpin configurations, with no antiparallel hydrogen bonded ladder for the $\beta 2$ and $\beta 3$ configurations persisting beyond the first 25 ps of the trajectory. The RMSD values of these $\beta$-hairpin simulations are again considerably higher than observed for $\varepsilon = r$ simulations (Table 3). For the $\alpha 4$ simulation, a similar picture emerged with loss of hydrogen bonds early in the trajectory and disappearance of an $\alpha$-helical hairpin structure. For the $\varepsilon = 80$ simulations, there is further evidence of the breakdown in secondary structure, as the percentage of core residues in the $\alpha$ and $\beta$ regions of the Ramachandran plot becomes equivalent except for $\beta 4$ (Table 3). In the $\alpha 4$ simulation, 28% of core residues from the SS2 part adopt a $\beta$-conformation, while in the $\beta 2$ and $\beta 3$ options, 20–25% core residues adopt an $\alpha$-conformation.

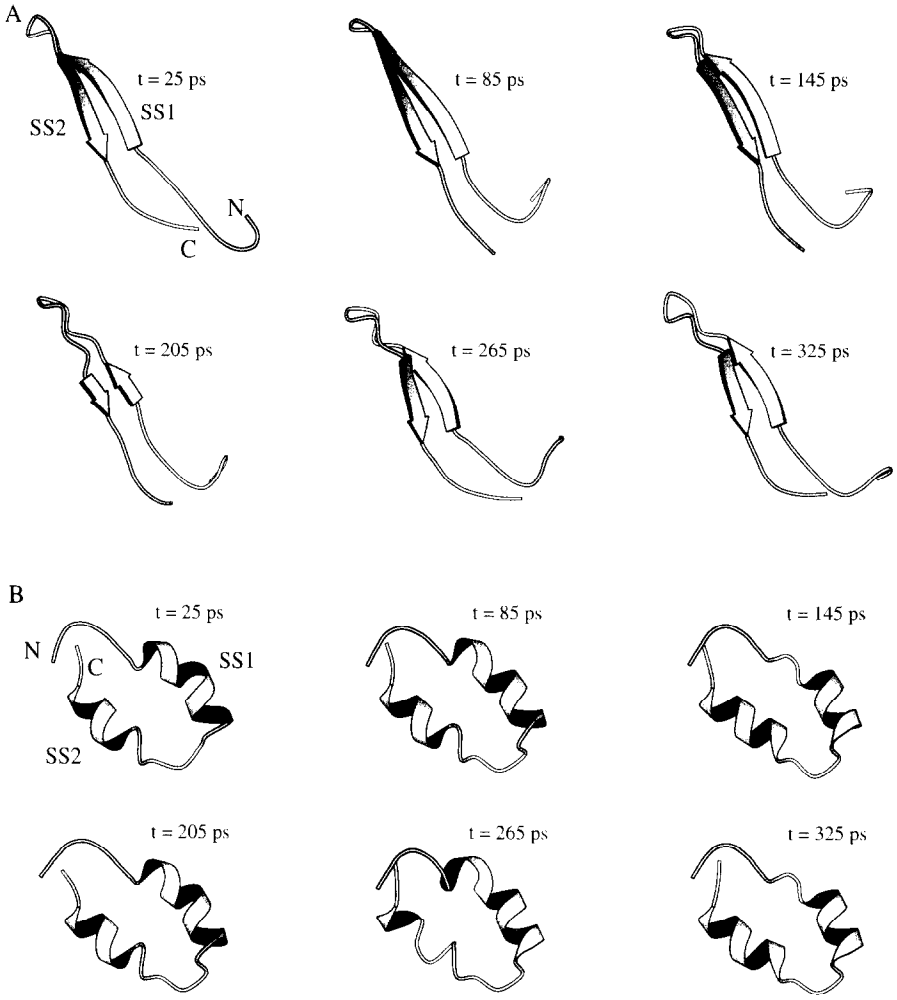


Fig. 4. Snapshots during molecular dynamics trajectory for $\beta 4$ (A) and $\alpha 4$ (B) with a distance-dependent dielectric. The structures are drawn as secondary structure representations using the program Molscript [22]. Secondary structure was defined using the DSSP algorithm within Rasmol.

### 3.7. Influence of the choice of initial model on MD simulations

To estimate the influence of the initial model on behaviour during subsequent MD simulations, we carried out multiple simulations for model $\beta 4$ with a distance-dependent dielectric, a simulation condition for which the initial configuration was well retained (Table 3). Accordingly, we selected three different structures from the $\beta 4$ ensemble with widely differ-

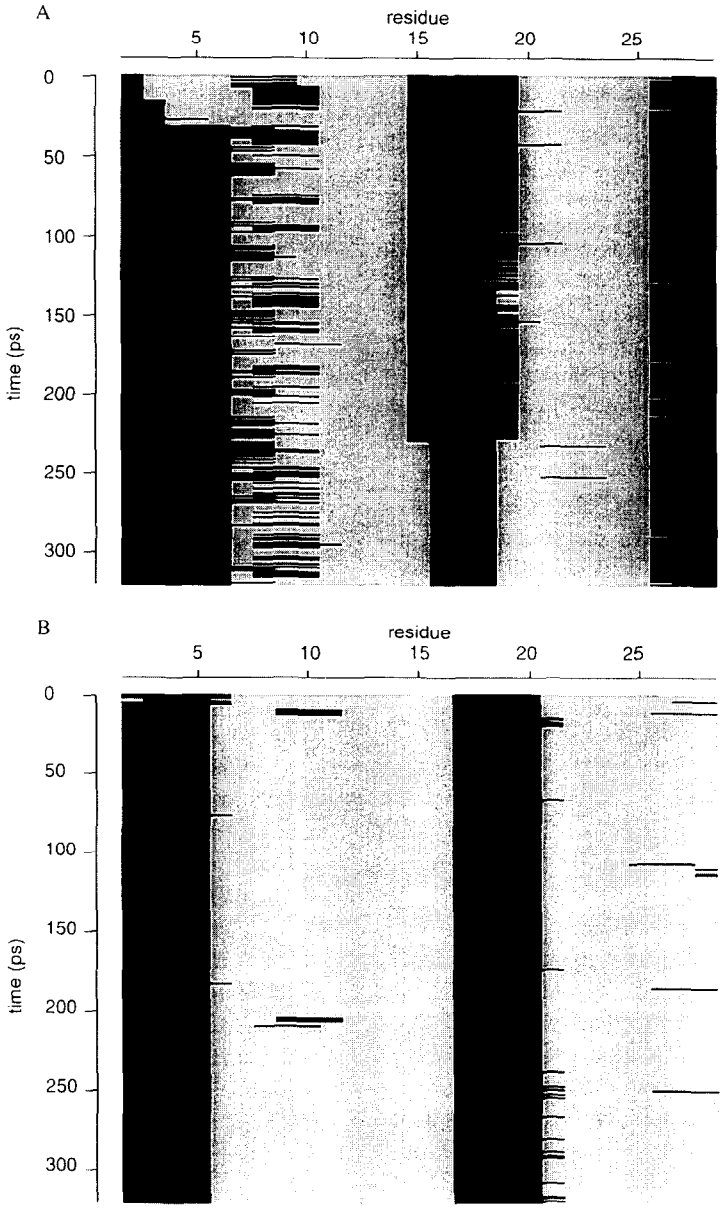


Fig. 5. Conformation of peptides during $\varepsilon = r$ simulations for $\beta 4$ (A) and $\alpha 4$ (B). The local conformation of the P-region peptide is shown at 1-ps intervals for the duration of the simulation. Black shading indicates random coil, while grey shading represents $\beta$-conformation in (A) and $\alpha$-conformation in (B). Conformation was assigned employing a three-residue window in which each residue in the window is required to be in the allowed region of the Ramachandran plot [23].

Table 4
Evaluation of choice of initial model on dynamics simulations

| | 'Core' region | | H-bond index |
|---|---|---|---|
| | $\alpha$ | $\beta$ | |
| High | 3 (3) | 75 (7) | 0.51 |
| Medium | 6 (3) | 76 (9) | 0.48 |
| Low | 21 (7) | 51 (6) | 0.18 |

Starting structures from the $\beta 4$ ensemble are defined with respect to their overall structural quality (high, medium and low). Conformational properties are defined and calculated as in Table 3.

ing stereochemical qualities, as assessed by Procheck [23]: 'high', 'medium' and 'low'. Their average secondary structure content during MD is presented in Table 4. Both conformational percentages and H-bonding indices are very close for the simulations with the 'high' and 'medium' stereochemical quality initial structures. The results are noticeably different for the simulation starting from the 'low' stereochemical quality model. Indeed, the $\alpha$-helical content increases at the expense of the $\beta$-conformation (final value ca. 50%). The markedly low H-bond indEx reflects such loss of $\beta$-hairpin configuration. However, one H-bond (adjacent to the turn) persisted throughout the simulation justifying the turn assignment. The data suggest that the starting model stereochemical quality influences the simulation only if the initial model exhibits poor stereochemistry.

## 4. Discussion

High-resolution three-dimensional structures are not yet determined for the vast majority of membrane proteins, in particular for ion channels. To aid our understanding of the conformations of such proteins, we have adopted a peptide approach to dissect out key fragments to estimate their local secondary structure and assay their functional properties [33]. It has already been shown that such fragments in isolation may adopt a conformation very similar to that within the intact protein [34], and that molecular modelling may be used to predict [24,35] structural features that can be subsequently tested by further experimentation. Here, we have attempted to represent our experimental structural data (circular dichroism and infrared) as geometric constraints for a peptide corresponding to the pore-forming region of the second domain of the electric eel voltage-gated sodium channel. After generating alternative possible models compatible with the spectroscopic data (i.e., three $\beta$-hairpins, $\beta 2$, $\beta 3$ and $\beta 4$, and an $\alpha$-helical hairpin $\alpha 4$), we examined their stability by means of MD simulations. One of the main limitations of these MD simulations is that they are performed in vacuo, i.e., in the absence of explicit solvent molecules. However, for a first approximation, we wished to test whether such MD simulations would reveal conformational preferences of the P-region, as the protocol was able to sample a larger conformational space than, e.g., energy minimisation. Thus, we hoped that the MD simulations might reveal whether or not models built on the basis of experimentally derived restraints were intrinsically stable.

For comparison with secondary structural data derived from our previous CD studies [18], four models were built for $P_{II}$ according to a restrained SA/MD protocol. Then, 300 ps of unrestrained MD simulations were run under three different dielectric constants. A comparable study has been described for the S4–S45 fragments from domains II and IV of the same channel [17]. CD results showed that the S45 moiety can undergo an $\alpha \rightarrow$ extended conformational change when increasing the medium polarity while S4 segments remain largely helical [36]. This is parallelled in independent ab initio modelling studies during which a loss of helicity for the S45 part is observed under the same conditions.

In the present study, we have used the persistence of secondary structure conformation as the criterion for assessing molecular dynamics simulations. This criterion identifies simulations starting from $\beta 4$ and $\alpha 4$ configurations and employing a distance-dependent dielectric constant as being preferred (Table 3). These simulations suggest that in isolation, the SS1 region of $P_{II}$ is more stable as an $\alpha$-helix than SS2, while the converse is true for a $\beta$-conformation. This suggestion is further supported by analysis of $\varepsilon = 2$ and $\varepsilon = 80$ simulations. In low dielectric medium (where $\beta$-conformation is not retained) the SS1 region of the $P_{II}$ peptide retains $\alpha$-helicity better than SS2, while in a high dielectric medium, the SS2 region of $\alpha 4$ loses $\alpha$-helicity in favour of $\beta$-confor-

mation. As regards the different turn probabilities for the β-hairpins, the 2-residue turn has a very constrained geometry, and the 3-residue turn seems disfavoured as described above. The 4-residue turn retains our preference since the H-bond near the turn persists significantly even for the simulation with the low stereochemical quality initial model (see Section 3.7).

In an apolar environment ($\varepsilon = 2$), the helical hairpin is preferred probably since H-bonds are all satisfied, whereas only half of the possible backbone H-bonds are formed in a β-hairpin in a monomeric state. However, many experimental points support inter-peptide association: (i) in CD experiments, increasing the peptide concentration promotes the β-conformational content [18]; and (ii) fluorescence energy transfer experiments carried out using similar peptides reveal a high propensity for self-recognition and assembly in lipid systems [19]. This, together with our own conductance measurements, suggest that the P-region peptide inserts into planar lipid bilayers and forms multimeric aggregates that fulfil the unsatisfied H-bonds of a monomeric β-hairpin. Given that experimental studies with the sodium channel P-peptides argue for tetrameric conducting aggregates [18] and with the help of methods for modelling transbilayer β-barrels [37], the next step will be to investigate possible configurations for these channel-forming aggregates.

On more general grounds, recent studies of interactions between helices or segments in membrane proteins [38,39], validated against membrane proteins of known three-dimensional structure lead us to hope that increasingly accurate models of ion channels will be formulated [40], while direct structural determinations remain somewhat elusive.

## Acknowledgements

This work was initiated, thanks to a grant from the Franco-British ALLIANCE programme. The Gdr 1153 CNRS 'Peptides et Protéines Amphipathiques' (HD), the Centre Régional Universitaire de Spectroscopie de Haute-Normandie, and the continuing support of the Wellcome Trust (MSPS) are also acknowledged.

## References

[1] A.L. Hodgkin, A.F. Huxley, J. Physiol. 116 (1952) 449.
[2] W.A. Catterall, Annu. Rev. Biochem. 64 (1995) 493.
[3] M. Noda, A. Shimizu, T. Tanabe, T. Takai, T. Kayano, T. Ikeda, H. Takahashi, H. Nakayama, Y. Kanaoka, N. Minamino, K. Kangawa, H. Matsuo, M.A. Raftery, T. Hirose, S. Inayama, H. Hayashida, T. Miyata, S. Numa, Nature 312 (1984) 121.
[4] D. Eisenberg, R.M. Weiss, T.C. Terwilliger, Nature 299 (1982) 371.
[5] W. Stühmer, F. Conti, X. Susuki, M. Wang, N. Noda, N. Yahagi, H. Kubo, S. Numa, Nature 339 (1989) 597.
[6] H. Terlau, S.H. Heinemann, W. Stühmer, M. Pusch, F. Conti, K. Imoto, S. Numa, FEBS Lett. 293 (1991) 93.
[7] S.H. Heinemann, H. Terlau, W. Stühmer, K. Imoto, S. Numa, Nature 356 (1992) 441.
[8] R.E. Greenblatt, Y. Blatt, M. Montal, FEBS Lett. 193 (1985) 125.
[9] S.R. Durell, H.R. Guy, Biophys. J. 62 (1992) 238.
[10] S.R. Durell, H.R. Guy, Neuropharmacology 35 (1996) 761.
[11] C. Sato, G. Matsumoto, J. Membr. Biol. 147 (1995) 45.
[12] M. Brullemans, O. Helluin, J.-Y. Dugast, G. Molle, H. Duclohier, Eur. Biophys. J. 23 (1994) 39.
[13] D.G. Doak, D. Mulvey, K. Kawaguchi, J. Villalain, I.D. Campbell, J. Mol. Biol. 258 (1996) 672.
[14] M.S.P. Sansom, I.D. Kerr, Protein Eng. 6 (1993) 65.
[15] H. Peled, Y. Shai, Biochemistry 33 (1994) 7211.
[16] M. Montal, Annu. Rev. Biophys. Biomol. Struct. 24 (1995) 31.
[17] P. Cosette, O. Helluin, J. Breed, Y. Pouny, Y. Shai, M.S.P. Sansom, H. Duclohier, in: V. Torre, F. Conti (Eds.), Neurobiology: Ion Channels, Neurons, and the Brain, Plenum, New York, 1996, p. 41.
[18] P. Cosette, L. Brachais, E. Bernardi, H. Duclohier, Eur. Biophys. J. 25 (1997) 275.
[19] Y. Pouny, Y. Shai, Biochemistry 34 (1995) 7712.
[20] A.T. Brünger, Yale Univ. Press, CT, 1992.
[21] B.R. Brooks, R.E. Bruccoleri, B.D. Olafson, D.J. States, S. Swaminathan, M. Karplus, J. Comp. Chem. 4 (1983) 187.
[22] P.J. Kraulis, J. Appl. Crystallogr. 24 (1991) 946.
[23] A.L. Morris, M.W. MacArthur, E.G. Hutchinson, J.M. Thornton, Proteins Struct. Funct. Genet. 12 (1992) 345.
[24] M. Nilges, A.T. Brünger, Protein Eng. 4 (1991) 649.
[25] M.S.P. Sansom, R. Sankararamakrishnan, I.D. Kerr, Nat. Struct. Biol. 2 (1995) 624.
[26] R.J. Loncharich, B.R. Brooks, Proteins Struct. Funct. Genet. 6 (1989) 32.
[27] C.-T. Zhang, K.-C. Chou, Biopolymers 41 (1997) 673.
[28] B.L. Sibanda, T.L. Blundell, J.M. Thornton, J. Mol. Biol. 206 (1989) 759.
[29] J.A. Schetz, P.A.V. Anderson, Biol. Bull. 185 (1993) 462.
[30] G.A. Jeffrey, W. Saenger, Springer, Berlin, 1991, p. 569.
[31] T.E. Creighton, 1993.
[32] R.A. Laskowski, D.S. Moss, J.M. Thornton, J. Mol. Biol. 231 (1993) 1049.

[33] H. Duclohier, O. Helluin, P. Cosette, A.R. Schoofs, S. Bendahhou, H. Wroblewski, Chemtracts, Biochem. Mol. Biol. 10 (1997) 189.
[34] I.L. Barsukov, D.E. Nolde, A.L. Lomize, A.S. Arseniev, Eur. J. Biochem. 206 (1992) 665.
[35] M. Nilges, A.T. Brünger, Proteins 15 (1993) 133.
[36] O. Helluin, J. Breed, H. Duclohier, Biochim. Biophys. Acta 1279 (1996) 1.
[37] M.S.P. Sansom, I.D. Kerr, Biophys. J. 69 (1995) 1334.
[38] F.A. Samatey, C. Xu, J.-L. Popot, Proc. Natl. Acad. Sci. U.S.A. 92 (1995) 4577.
[39] M.S.P. Sansom, H.S. Son, R. Sankararamakrishnan, I.D. Kerr, J.B. Breed, Biophys. J. 68 (1995) 1295.
[40] M. Montal, Curr. Opin. Struct. Biol. 5 (1995) 501.